Revisiting absolute amplitude matching in waveform inversion

Xukai Shen

ABSTRACT

In waveform inversion, the high resolution in the inversion results are usually attributed to absolute amplitude matching. Such high resolution is particularly attractive in complex geological settings where conventional ray-based methods fail to deliver enough resolution. In this paper, I reexamine the importance of absolute amplitude matching in waveform inversion. With enough illumination angles, absolute amplitude matching does not bring additional resolution, yet makes the inversions result extremely sensitive to absolute amplitude mismatches. I illustrate this with acoustic inversions of non-acoustic data.

INTRODUCTION

In recent years, exploration geophysicists have gradually recognized that by using finite-frequency seismic wave propagation, waveform inversion (Tarantola, 1984; Pratt et al., 1998; Mora, 1987) tends to give more accurate velocity estimations (Ravaut et al., 2004; Sheng et al., 2006; Sirgue et al., 2009) than those from ray-based methods (Hampson and Russell, 1984; Olson, 1984; White, 1989). Using waveform inversion for velocity estimation is particularly beneficial in geologically complex areas. In such areas, complex velocity can cause serious problems for imaging target regions, unless the overburden velocity is accurately estimated. It is also in those geological setting where finite-frequency wave propagation in waveform inversion works much better than high-frequency asymptotic rays.

The major benefit of waveform inversion results over ray-based inversion results is the resolution. Generally waveform inversion results have much higher resolution than ray-based inversion results. This is usually attributed to the absolute amplitude matching carried out in minimizing the conventional waveform inversion objective function. Such theory can explain the near-perfect results in most synthetic waveform inversions. But it cannot explain the high-resolution results in real data applications (Sirgue et al., 2009). In those applications, computational constraints have mandated the use of the acoustic wave-equation in the inversion engine, yet real data contains a lot of non-acoustic phenomena. These two facts make it extremely difficult to match the absolute amplitude of the synthetic data modeled from the acoustic wave-equation to those of the recorded data, even when the correct near-surface model is given.

In this paper, I revisit the importance of the absolute amplitude matching in realistic waveform inversions. To simulate practical applications, I perform acoustic inversions where data are generated using non-acoustic wave-equations. The importance of the absolute amplitude matching is investigated by using both conventional objective function(Tarantola, 1984) and kinematic based objective function(Shen, 2010) in the inversions. The conventional objective function aims at full amplitude matching between observed data and modeled data. The kinematic based objective function de-emphasizes amplitude matching and focuses more on phase matching. I compare inversion results from using the two objective functions to determine the importance of the absolute amplitude matching in realistic applications of waveform inversion. The paper is organized as follows: First, I briefly revisit the kinematic based objective function, and explain why it focuses mainly on phase matching. Then I compare the inversion results using elastic data modeled from a realistic earth model. Finally, I draw some conclusions on the importance of amplitude matching in practical waveform inversion.

KINEMATIC BASED OBJECTIVE FUNCTION

The generalized waveform inversion objective function can be written as

$$f\left(\mathbf{d_{obs}}, \mathbf{D(m)}\right) \approx \mathbf{0}, \tag{1}$$

where f is a function of $\mathbf{d_{obs}}$, the observed data, and $\mathbf{D(m)}$ is the forward-modeled synthetic data from $\mathbf{m}$, the velocity model. Observed data can be in either the frequency domain or the time domain, depending on the actual form of $\mathbf{f}$. For example, if we take $\mathbf{f}$ as the L2 norm of $(\mathbf{d_{obs}} - \mathbf{D(m)})$, we obtain the objective function of conventional waveform inversion (Tarantola, 1984; Pratt et al., 1998); if we take $\mathbf{f}$ as the L2 norm of the natural logarithm of $\mathbf{D(m)}/\mathbf{d_{obs}}$, we obtain the so-called logarithmic objective function of waveform inversion (Shin and Min, 2006). The kinematic based objective function takes the following form of $\mathbf{f}$:

$$\begin{aligned} f &= \sum_{\mathbf{s},\mathbf{r}} \|\mathbf{r(s,r)}\|^{\mathbf{2}} \\ &= \sum_{\mathbf{s},\mathbf{r}} \left\| \frac{\mathbf{D(s,r,m)}}{\sqrt{\mathbf{D^T(s,r,m)D(s,r,m)}}} - \frac{\mathbf{d_{obs}(s,r)}}{\sqrt{\mathbf{d_{obs}^T(s,r)d_{obs}(s,r)}}} \right\|^{\mathbf{2}}, \end{aligned} \tag{2}$$

where $\mathbf{m}$ is the model, which consists of near-surface velocity; $\mathbf{d_{obs}}$ are traces of recorded early-arrivals after band-passing; $\mathbf{D}$ are band-passed synthetic early-arrival traces modeled with the constant-density two-way acoustic wave-equation operator, from near-surface velocity; $\mathbf{s}$ and $\mathbf{r}$ are source and receiver locations, respectively. The notation $\|\mathbf{a}\|$ denotes the L2 norm, or the energy, of trace $\mathbf{a}$.

Geophysical Interpretations of the Objective Function

In the new objective function, I weight both the recorded data and the forward-modeled data by their RMS energy, trace by trace. This ensures that recorded data and forward-modeled data have approximately the same relative amplitudes, and that waveform inversion in this case will focus more on phase comparison. This is particularly obvious if there is only one arrival in both recorded data and observed data, in which case we can use both monochromatic recorded data and monochromatic observed data expressed in the frequency domain, i.e., assuming:

$$\begin{aligned}\mathbf{d_{obs}}(\mathbf{s},\mathbf{r}) &= \mathbf{A_{obs}} \exp\left(\mathbf{i}\omega \mathbf{t_{obs}}(\mathbf{s},\mathbf{r})\right)\\ \mathbf{D}(\mathbf{s},\mathbf{r},\mathbf{m}) &= \mathbf{A_D} \exp\left(\mathbf{i}\omega \mathbf{t_D}(\mathbf{s},\mathbf{r},\mathbf{m})\right).\end{aligned} \tag{3}$$

Equation 2 then becomes

$$\begin{aligned}f &= \sum_{\mathbf{s},\mathbf{r}} \|\mathbf{r}(\mathbf{s},\mathbf{r})\|^{\mathbf{2}}\\ &= \| \exp\left(\mathbf{i}\omega \mathbf{t_D}(\mathbf{s},\mathbf{r},\mathbf{m})\right) - \exp\left(\mathbf{i}\omega \mathbf{t_{obs}}(\mathbf{s},\mathbf{r})\right) \|^{\mathbf{2}},\end{aligned} \tag{4}$$

which explicitly states that, for a single frequency of a single event, the objective function is performing phase comparison of the specific frequency. This phase comparison becomes an approximation for band-limited data with multiple events. Yet in such cases, the objective function still heavily emphasizes phase comparison. This can also be seen by expanding equation 2:

$$\begin{aligned}f &= \left\| \frac{\mathbf{D}(\mathbf{s},\mathbf{r},\mathbf{m})}{\sqrt{\mathbf{D^T}(\mathbf{s},\mathbf{r},\mathbf{m})\mathbf{D}(\mathbf{s},\mathbf{r},\mathbf{m})}} - \frac{\mathbf{d_{obs}}(\mathbf{s},\mathbf{r})}{\sqrt{\mathbf{d_{obs}^T}(\mathbf{s},\mathbf{r})\mathbf{d_{obs}}(\mathbf{s},\mathbf{r})}} \right\|^{\mathbf{2}}\\ &= \left(\frac{\mathbf{D}}{\sqrt{\mathbf{D^T D}}} - \frac{\mathbf{d_{obs}}}{\sqrt{\mathbf{d_{obs}^T d_{obs}}}} \right)^{\mathbf{T}} \left(\frac{\mathbf{D}}{\sqrt{\mathbf{D^T D}}} - \frac{\mathbf{d_{obs}}}{\sqrt{\mathbf{d_{obs}^T d_{obs}}}} \right)\\ &= \left(\frac{\mathbf{D}}{\|\mathbf{D}\|} - \frac{\mathbf{d_{obs}}}{\|\mathbf{d_{obs}}\|} \right)^{\mathbf{T}} \left(\frac{\mathbf{D}}{\|\mathbf{D}\|} - \frac{\mathbf{d_{obs}}}{\|\mathbf{d_{obs}}\|} \right)\\ &= \frac{\mathbf{D^T}}{\|\mathbf{D}\|}.\frac{\mathbf{D}}{\|\mathbf{D}\|} - \frac{\mathbf{d_{obs}^T}}{\|\mathbf{d_{obs}}\|}.\frac{\mathbf{D}}{\|\mathbf{D}\|} - \frac{\mathbf{D^T}}{\|\mathbf{D}\|}.\frac{\mathbf{d_{obs}}}{\|\mathbf{d_{obs}}\|} + \frac{\mathbf{d_{obs}^T}}{\|\mathbf{d_{obs}}\|}.\frac{\mathbf{d_{obs}}}{\|\mathbf{d_{obs}}\|}\\ &= \mathbf{2} - \frac{\mathbf{D^T}}{\|\mathbf{D}\|}.\frac{\mathbf{d_{obs}}}{\|\mathbf{d_{obs}}\|}\\ &= \mathbf{2} - \frac{\mathbf{D}(\mathbf{s},\mathbf{r},\mathbf{m})}{\sqrt{\mathbf{D^T}(\mathbf{s},\mathbf{r},\mathbf{m})\mathbf{D}(\mathbf{s},\mathbf{r},\mathbf{m})}}.\frac{\mathbf{d_{obs}}(\mathbf{s},\mathbf{r})}{\sqrt{\mathbf{d_{obs}^T}(\mathbf{s},\mathbf{r})\mathbf{d_{obs}}(\mathbf{s},\mathbf{r})}}.\end{aligned} \tag{5}$$

Equation 5 shows that minimizing the objective function is equivalent to maximizing the correlation between weighted observed data and weighted modeled data. Since the correlation is weighted, the maximization is achieved by aligning corresponding events-another way of minimizing kinematic errors between observed data and modeled data. A similar objective function has been proved to be robust in real data application (Routh et al., 2011).

ACOUSTIC INVERSION OF ELASTIC DATA

Here I perform waveform inversion using recorded elastic data modeled from a realistically complex earth model. To better understand the inversion results, I first examine the differences in modeled data between the acoustic wave equation and the elastic wave equation. Then I perform inversion with different objective functions to determine the importance of absolute amplitude matching in such inversion scenarios.

Model and survey description

The true P-wave velocity model (Figure 1 top panel) is generated by a series of geological processes. The details of generating the model for the inversion are described in Shen (2013). The S-wave velocity is created by using a typical near-surface Vp/Vs ratio (Figure 1 middle panel). The density model is created from the Vp model using the Gardner equation (Gardner et al., 1974) (Figure 1 bottom panel). Due to the extremely slow S-wave velocity in the very near surface, Vp, Vs and density models require 5-m spatial sampling in both x and z to avoid spatial dispersion, and the modeling time step is 0.5 ms to assure stability. A total of 100 shots were modeled with 100-m shot sampling. Receivers are everywhere on the surface for each shot. The recorded data are the pressure wavefield at the receiver locations.

Forward modeling comparison

The goal of the acoustic inversions here is to recover the low velocity structures from elastic data, which include a low velocity layer in the mid depth, and a low velocity erosion to the left. As a result, it is important to understand which part of the data is associated with the low velocity structures, and how the acoustic data from the low velocity structures differs from the corresponding elastic data.

A typical elastically modeled shot gather from the true model is shown in Figure 3. The elastic modeling did not use free surface boundary condition, hence no strong surface wave exist in the shot gather. To identify the part of the data that corresponds to the low velocity structures, an elastic shot (Figure 4) with the same geometry and source wavelet is modeled from the same model without the low velocity structures (Figure 2). Comparing the two shot gather, it is obvious that the reflections from the top and bottom of the low velocity layer will be the driving force for recovering the low velocity layer. Yet before performing acoustic inversion, another shot gather with the same geometry and wavelet was modeled using the true p-wave velocity model, with the acoustic wave equation. Compare this acoustic shot gather with the elastic shot gather from the true model (Figure 5), the reflection data from the low velocity layer have very similar kinematics in both shot gathers.

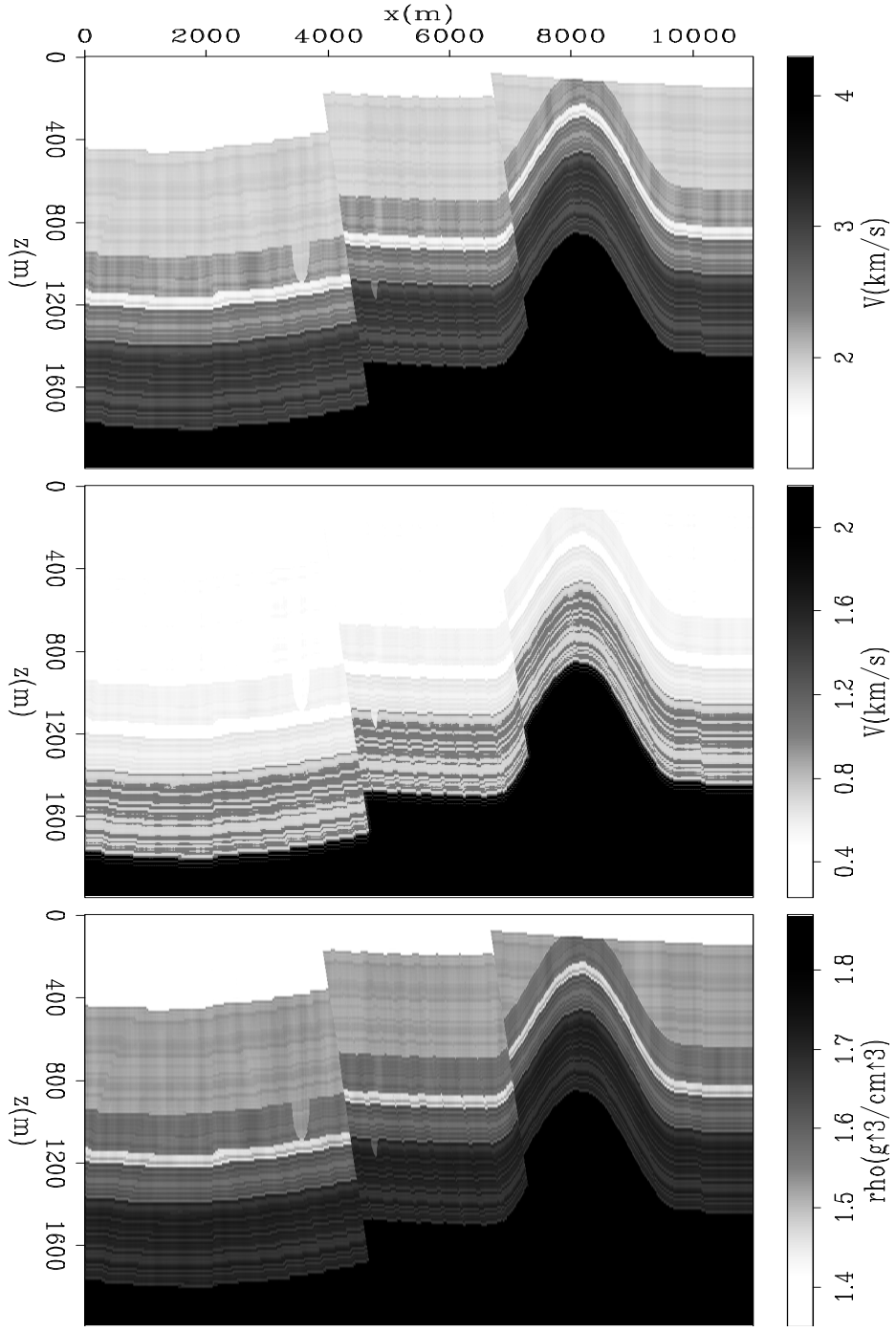

Figure 1: True earth model created by geological process, top:P-wave velocity; middle:S-wave velocity; bottom:density. [**CR**]

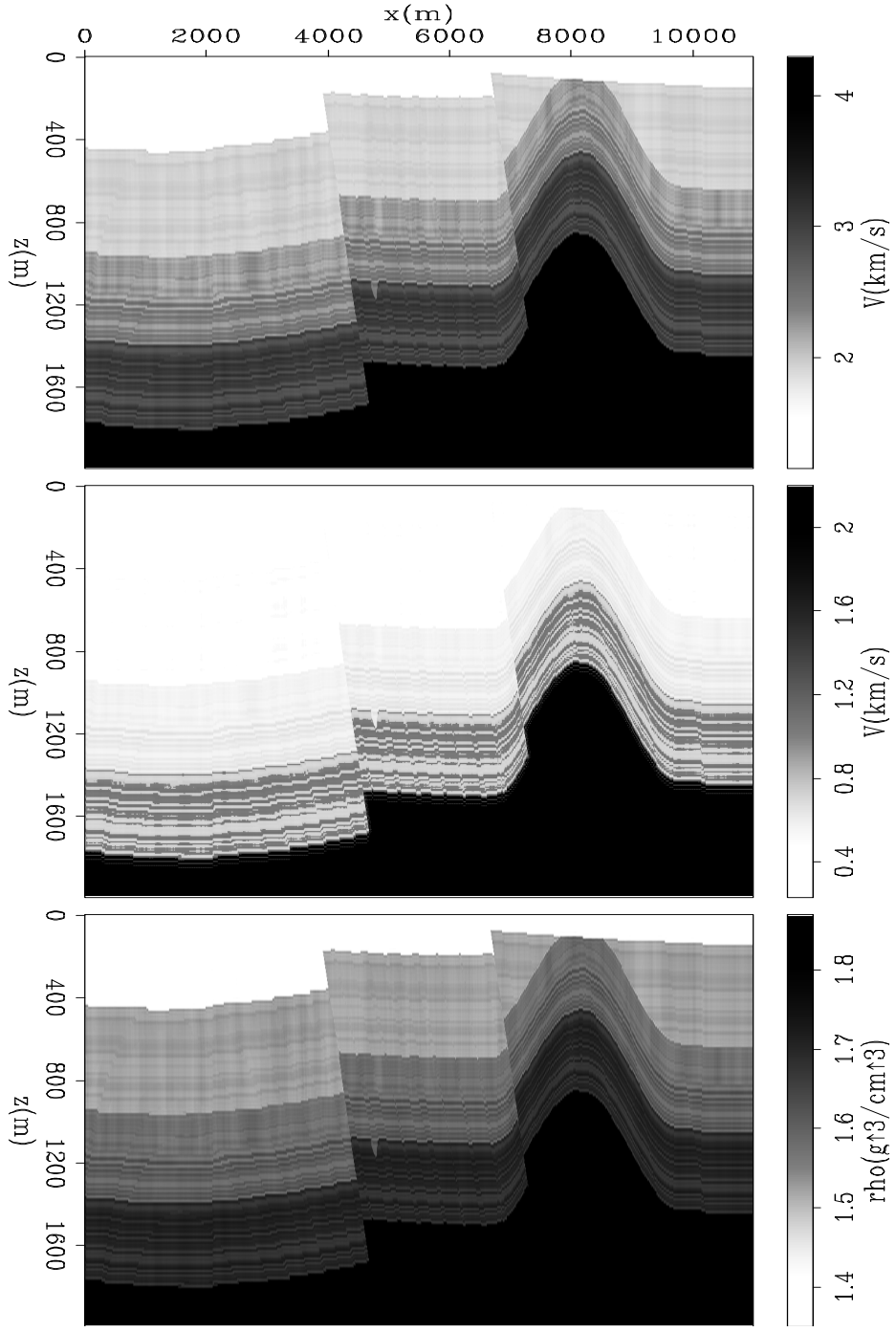

Figure 2: True earth model without the low velocity structures, top:P-wave velocity; middle:S-wave velocity; bottom:density. [**CR**]

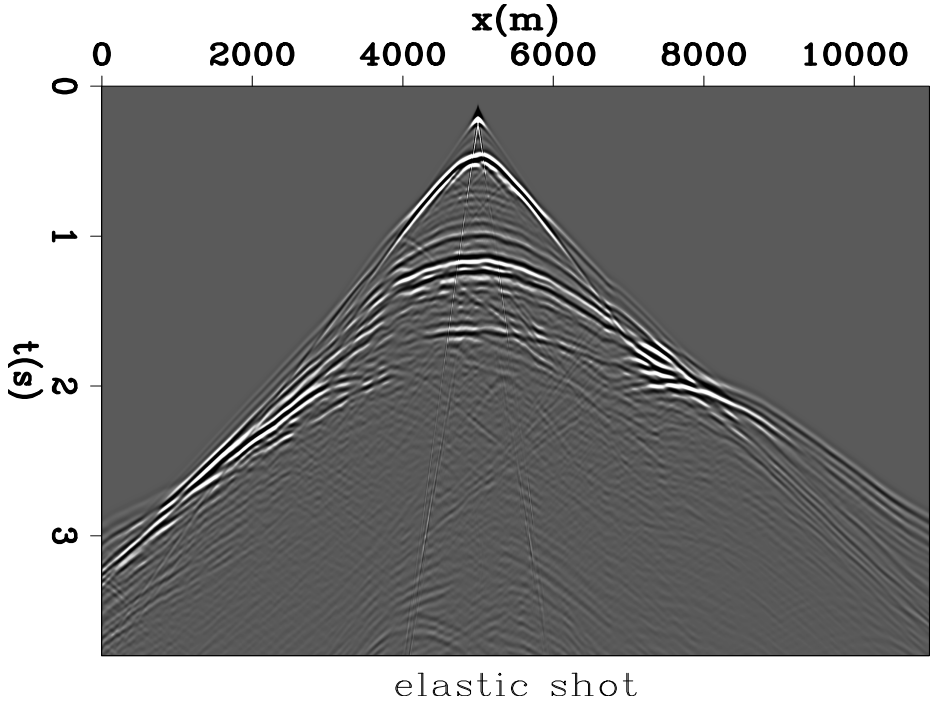

Figure 3: Elastic shot gather modeled from the true earth model. [**CR**]

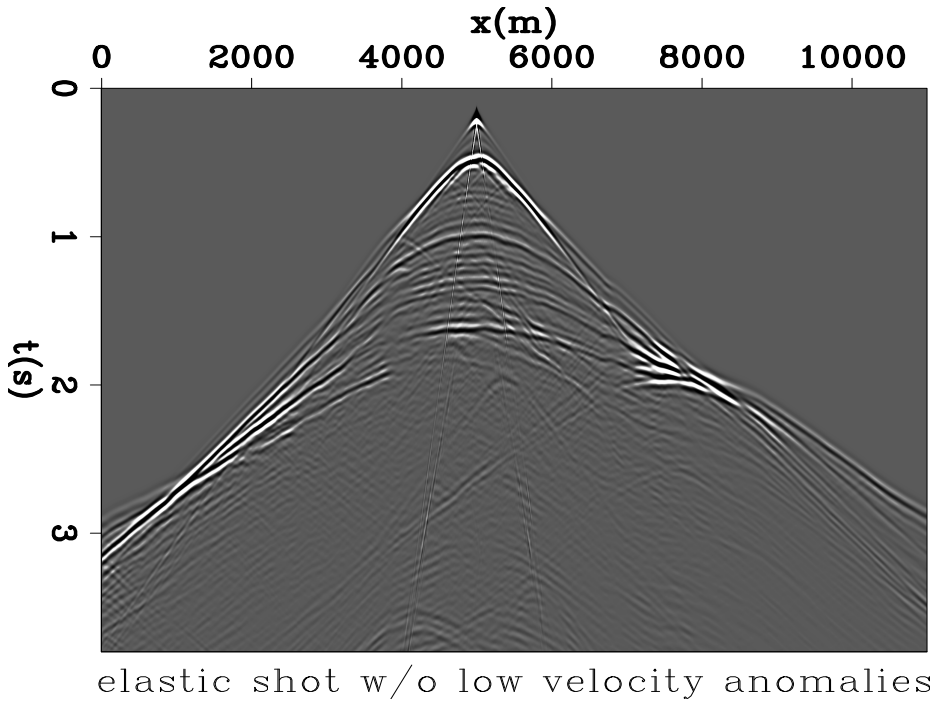

Figure 4: Elastic shot gather modeled from the earth model without the low velocity structures. [**CR**]

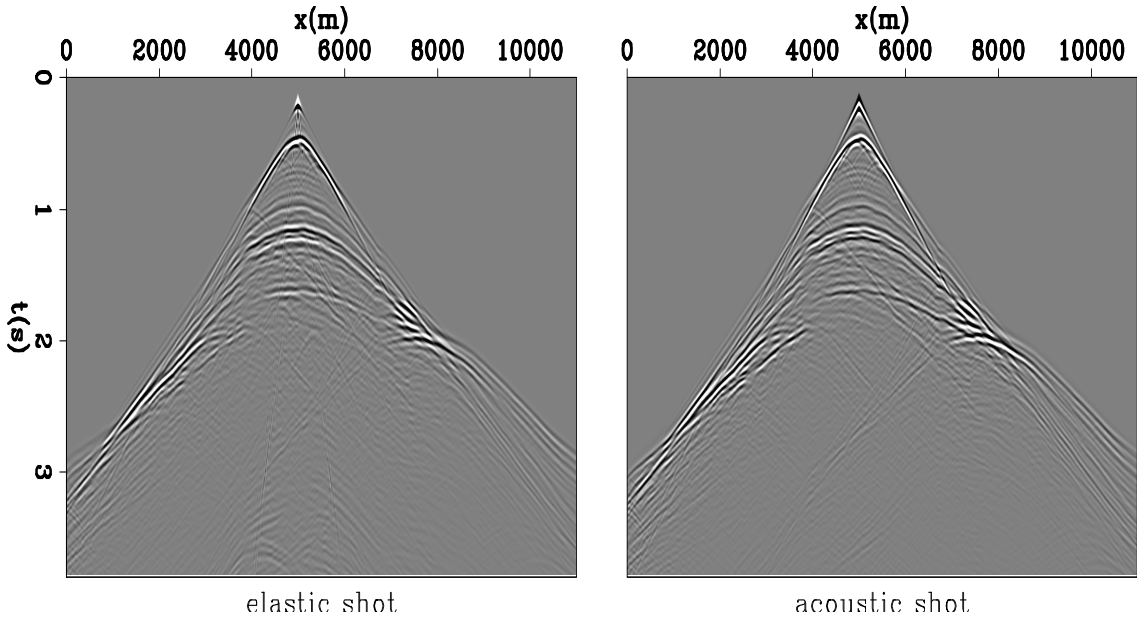

Figure 5: Side by Side comparison of elastic shot gather modeled from the true earth model and acoustic shot gather modeled from the true p-wave velocity model. [**CR**]

Inversion comparison

For waveform inversion, the modeled elastic data were lowpass filtered with 6Hz cut-off frequency. Also to simulate realistic scenario, near-offset data were not used for inversion. After bandpass and windowing, The same shot in Figure 3 become the one in Figure 6. The starting model was also built with the same geological process with exclusions of the details of the model (Figure 7). The low velocity structures were excluded, and the thin layers within each deposited layer were also excluded. Several inversions were run. The first inversion is the one using the kinematic based objective function described earlier. All the other inversions use the conventional L2 objective function, with different scaling factors used for the source wavelet as input. In each of the inversions, the source wavelets are exactly the same for all the shots. The scale only changes between different inversions.

The inversion result from using the kinematic based objective function recovers the low velocity structures well (Figure 8 and 9). Not only are the depth and the lateral locations accurate, but also are the lateral continuity of the low velocity structures well resolved. Most of the fine layers are not resolved, which is understandable due to the low frequency content of the input data. Residual-wise, the objective function value decreased significantly (Figure 10) after the inversion. The data residual of the shot gather shown in Figure 6 also decreased significantly after the inversion (Figure 11). Such improvements result from the good kinematic matching between input data and modeled data (Figure 12) after the inversion. More specifically, the top and the bottom reflections from the low velocity layer in the final modeled data matches those

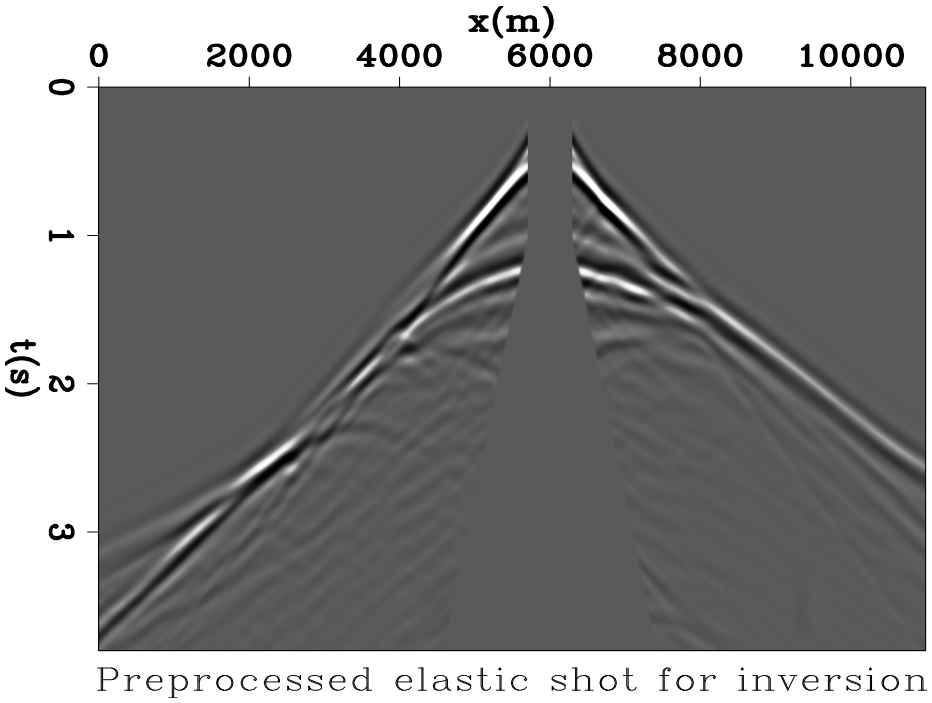

Figure 6: Input elastic shot gather for the waveform inversions. [**CR**]

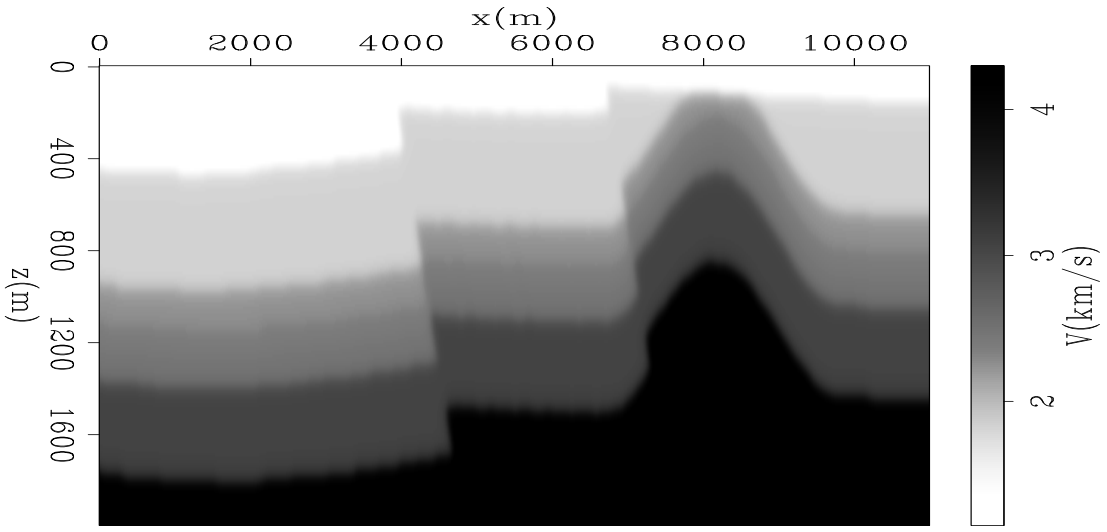

Figure 7: Initial velocity model for the waveform inversions. [**CR**]

in the input data very well.

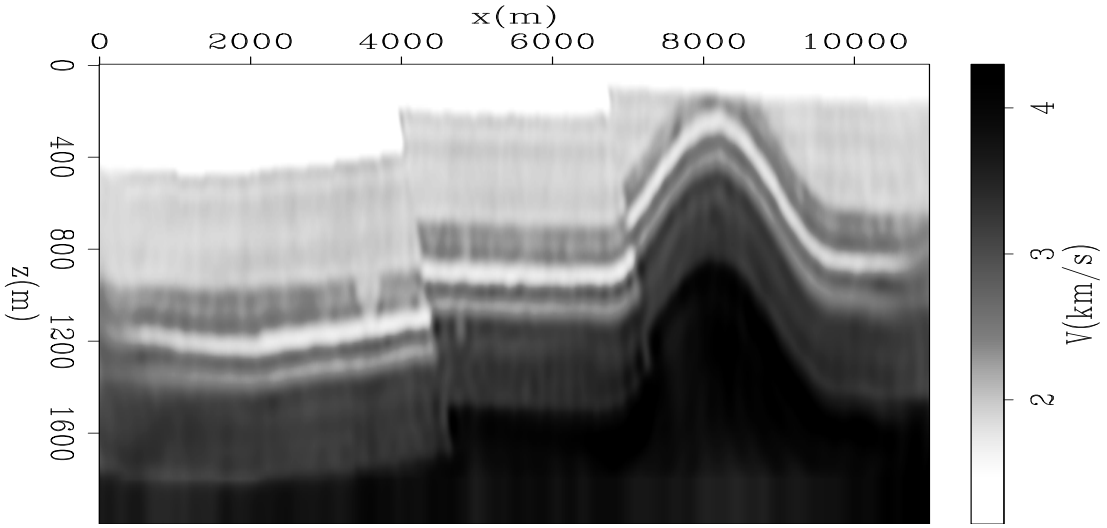

Figure 8: Waveform inversion result using the kinematic based objective function. [**CR**]

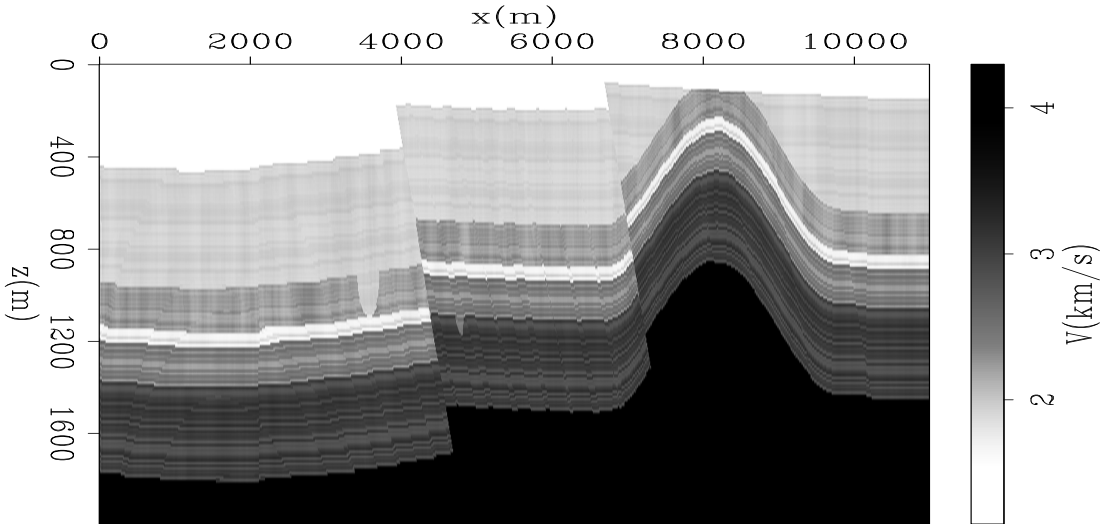

Figure 9: True p-wave velocity model. [**CR**]

Given the good inversion result from using the kinematic based objective function. The ratio of energy between final modeled data and observed data were calculated, and is used as one of the source wavelet scaling factor for the subsequent inversions using the conventional L2 objective function. This scaling factor is denoted as the base scaling factor, the other scaling factors are distributed around this base factor, with some larger ones and some smaller ones. Inversion result from using the source wavelet scaled by the base factor (Figure 13) did not resolve the low velocity structures well. The lateral continuity of the low velocity layer is not recovered, and the low

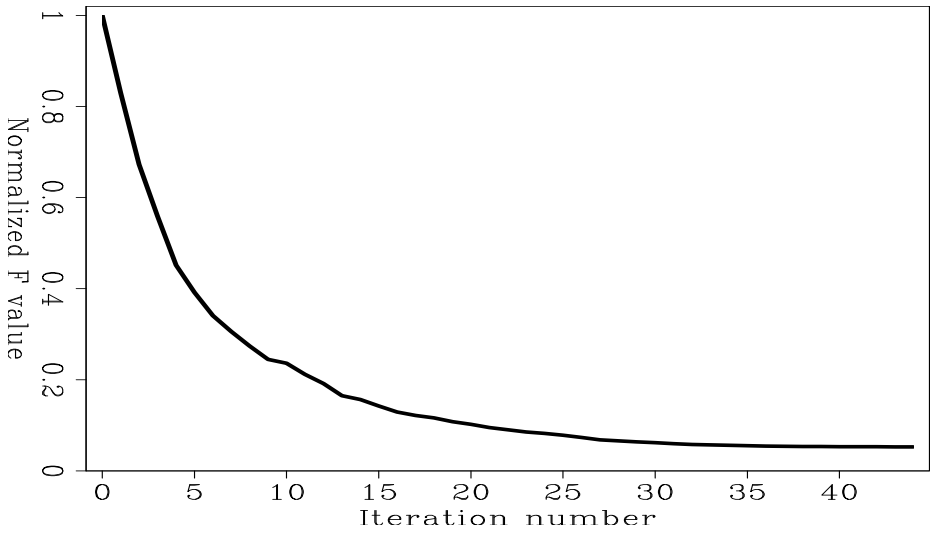

Figure 10: Objective function value of the kinematic based waveform inversion. [**CR**]

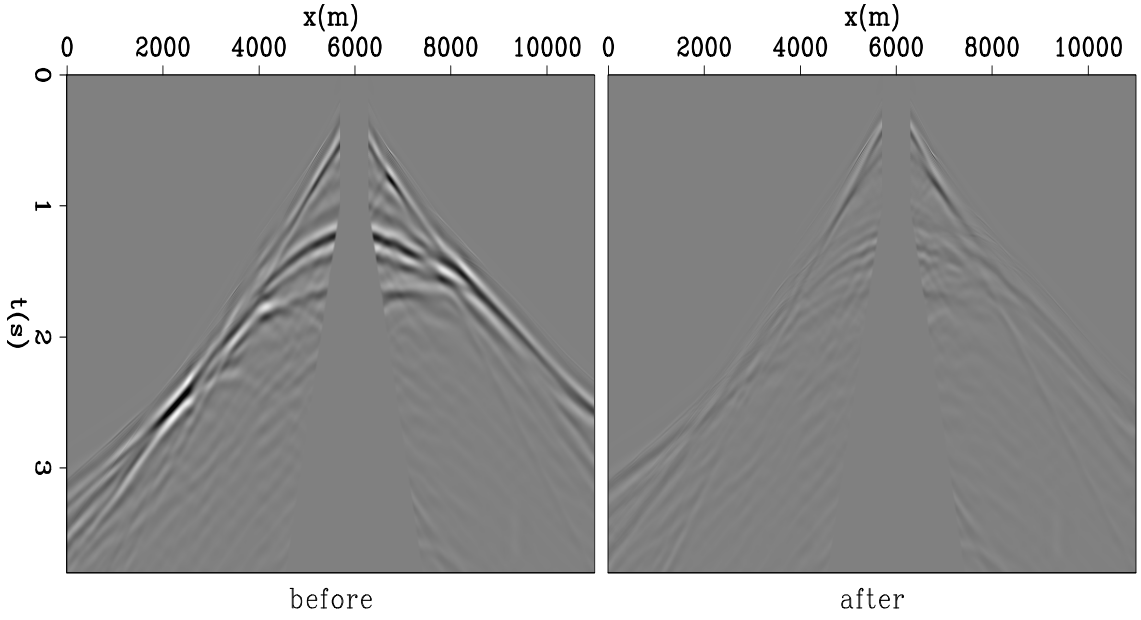

Figure 11: Shot gather data residual before and after the kinematic based waveform inversion. [**CR**]

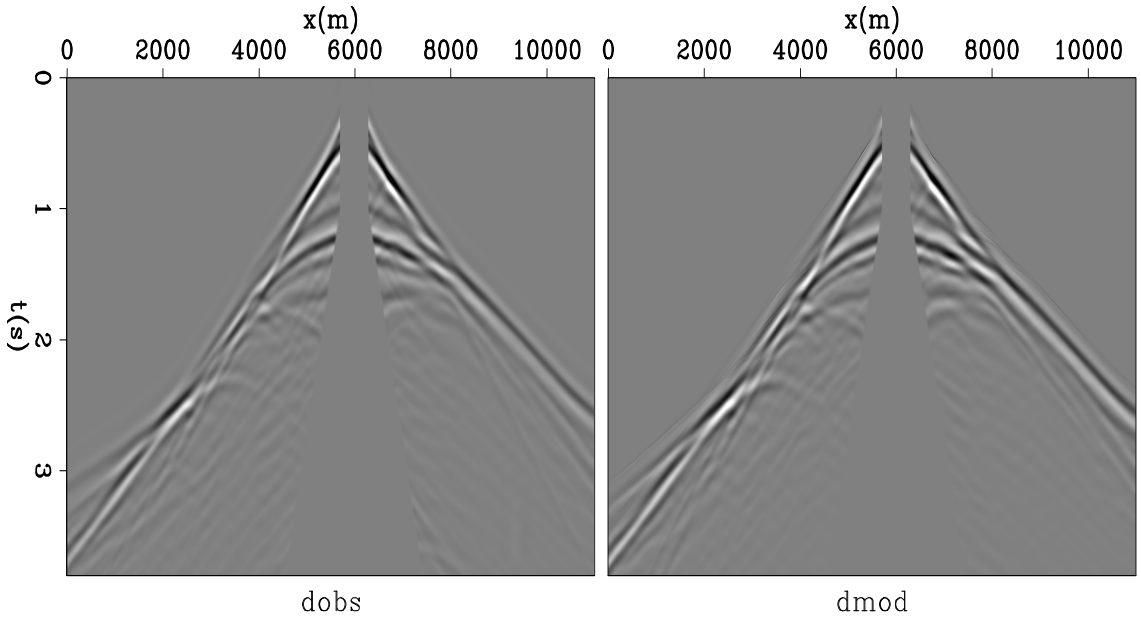

Figure 12: Comparison of input data and final modeled data from the kinematic based waveform inversion result. [**CR**]

velocity erosion to the left is put at a depth too shallow. Increase the scaling factor makes matter even worse (Figure 14). Only when the scaling factor is significantly decreased (by 40% in this case), does the inversion result looks reasonable (Figure 15). However, close examination of the result reveals that the low velocity layer is slightly deeper than its true depth, and the bottom of the low velocity erosion to the left was not well resolved. Data-fitting wise, the objective function values actually decreased more in the case of using the base scaling factor (Figure 16). In fact, the objective function value only goes down about 60% before flattening out (Figure 17) in the case of using the small scaling factor. Comparing input data with final modeled data in both cases, it become evident that with the small scaling factor, final modeled data have better kinematic matching (Figure 19), while with the base scaling factor, amplitude matching become better at the expense of the kinematic matching (Figure 18).

In summary, to correctly resolve velocity structures, it is more important to match the kinematics of the input data. While matching amplitude can potentially be beneficial, it is dangerous to match amplitude in practical inversions. More specifically, amplitude matching tend to take precedence over kinematic matching, if we are to use conventional L2 objective function, unless a proper scaling factor can be found for the input source wavelets. Since there is no easy way of finding the scaling factor, practical use of the conventional L2 objective function in waveform inversion is challenging.

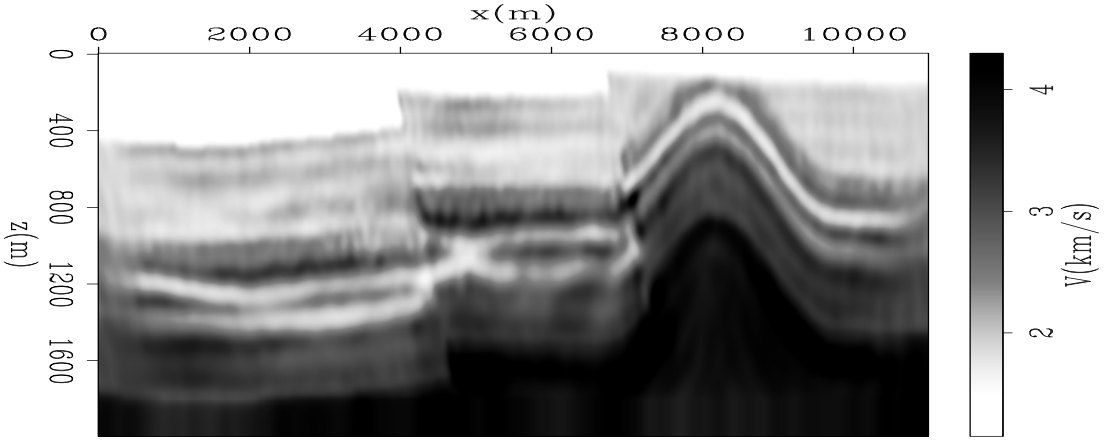

Figure 13: Waveform inversion result using the conventional L2 objective function, with the base scaling factor. [**CR**]

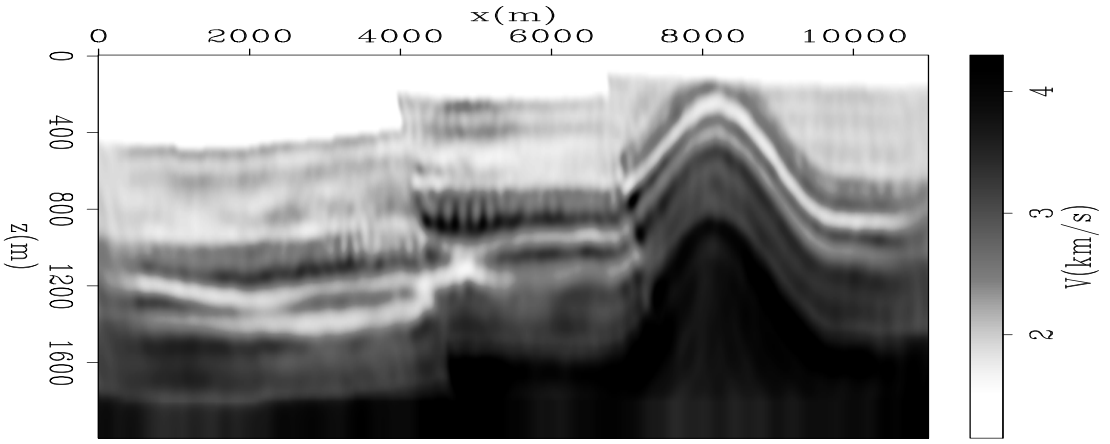

Figure 14: Waveform inversion result using the conventional L2 objective function, with the large scaling factor. [**CR**]

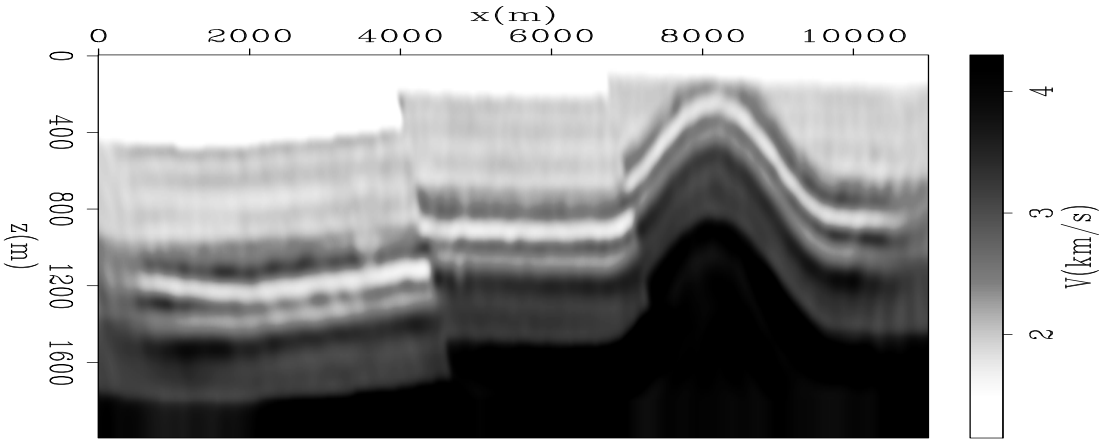

Figure 15: Waveform inversion result using the conventional L2 objective function, with the small scaling factor. [**CR**]

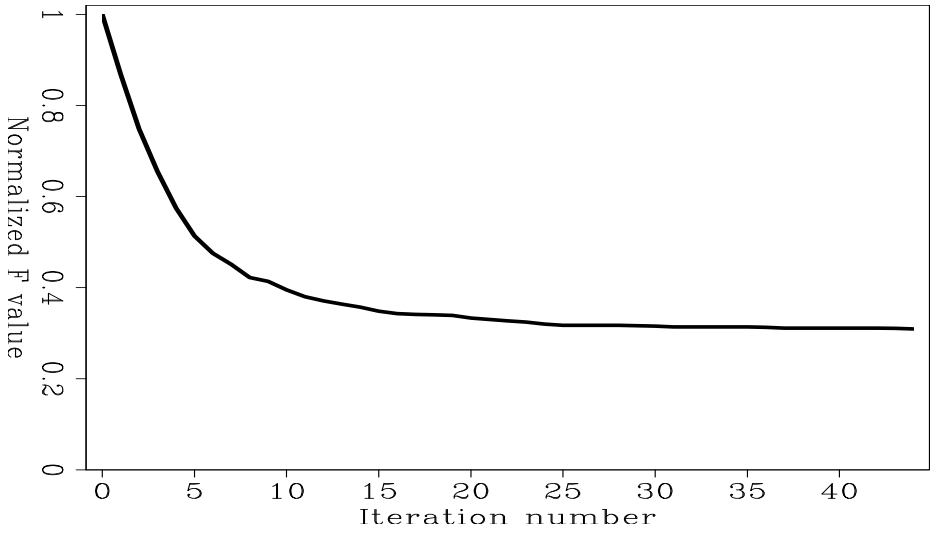

Figure 16: Objective function value of the conventional L2 waveform inversion, with the base scaling factor. [**CR**]

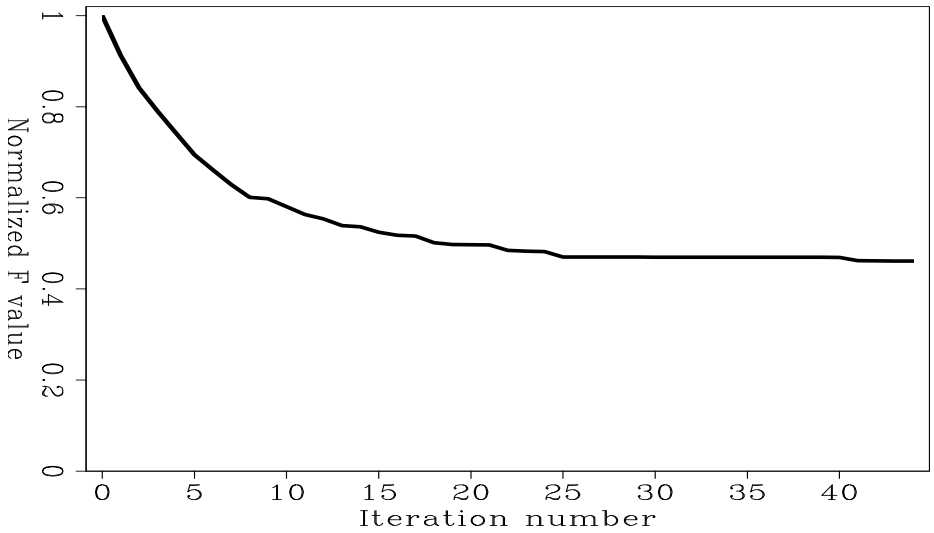

Figure 17: Objective function value of the conventional L2 waveform inversion, with the small scaling factor. [**CR**]

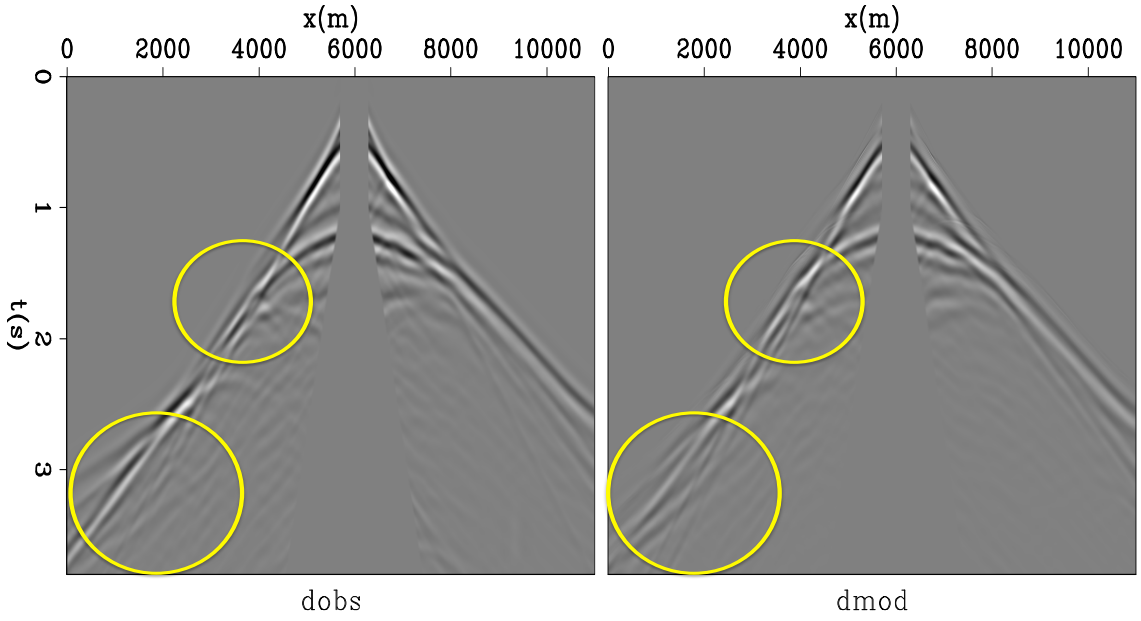

Figure 18: Comparison of input data and final modeled data from the conventional L2 waveform inversion result, with the large scaling factor. Yellow circles indicate where kinematic matchings are bad. [**CR**]

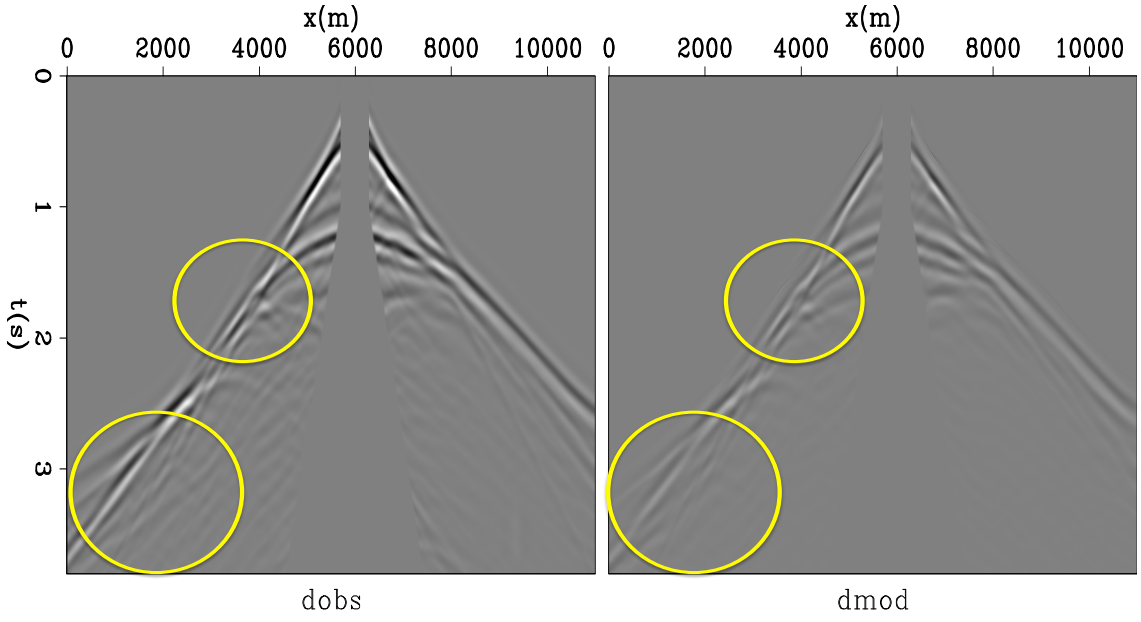

Figure 19: Comparison of input data and final modeled data from the conventional L2 waveform inversion result, with the small scaling factor. Yellow circles indicate where kinematic matchings are good. [**CR**]

CONCLUSIONS

Waveform inversion can provide high-resolution velocity models. In the case of complex earth models, data usually illuminate the subsurface well enough, hence the inversion results using kinematic based objective function have high resolution. With conventional L2 objective function, it is dangerous to use acoustic inversion for elastic input data. In such cases, amplitude matching dominates the inversion and damages kinematic matching, results in bad inversion results. On the other hand, using kinematic based objective function, acoustic inversion of elastic input data gives much better results.

REFERENCES

Gardner, G. H. F., L. W. Gardner, and A. R. Gregory, 1974, Formation velocity and density-the diagnostic basics for stratigraphic traps: Geophysics, **39**, 770–780.

Hampson, D. and B. Russell, 1984, First-break interpretation using generalized linear inversion: Journal of CSEG, **20**, 40–54.

Mora, P., 1987, Elastic wavefield inversion: SEP Ph.D Thesis.

Olson, K. B., 1984, A stable and flexible procedure for the inverse modelling of seismic first arrivals: Geophysical Prospecting, **37**, 455–465.

Pratt, R. G., C. Shin, and G. Hicks, 1998, Gauss-Newton and full Newton methods in frequency domain seismic waveform inversion: Geophysical Journal International, **133**, 341–362.

Ravaut, C., S. Operto, L. Improta, J. Virieux, A. Herrero, and P. Dell'Aversana, 2004, Multiscale imaging of complex structures from multifold wide-aperture seismic data by frequency-domain full-waveform tomography: application to a thrust belt: Geophysical Journal International, **159**, 1032–1056.

Routh, P., J. Krebs, S. Lazaratos, A. Baumstein, I. Chikichev, N. Downey, S. Lee, D. Hinkley, and J. Anderson, 2011, Full-wavefield inversion of marine streamer data with the encoded simultaneous source method: EAGE 73th Conference.

Shen, X., 2010, Near-surface velocity estimation by weighted early-arrival waveform inversion: SEG Expanded Abstracts.

———, 2013, Near-surface velocity estimation for a realistic 3d synthetic model: SEP Report, **150**.

Sheng, J., A. Leeds, M. Buddensiek, and G. T. Schuster, 2006, Early arrival waveform tomography on near-surface refraction data: Geophysics, **71**, U47–U57.

Shin, C. and D. J. Min, 2006, Waveform inversion using a logarithmic wavefield: Geophysics, **71**, R31–R42.

Sirgue, L., O.I.Barkved, J. V. Gestel, O. Askim, and R. Kommedal, 2009, 3d waveform inversion on valhall wide-azimuth obc: EAGE 71th Conference.

Tarantola, A., 1984, Inversion of seismic reflection data in the acoustic approximation: Geophysics, **49**, 1259–1266.

White, D. J., 1989, Two-dimensional seismic refraction tomogaphy: Geophysical Journal International, **97**, 223–245.